Journal of Mechanical and Electrical Intelligent System (JMEIS)

Research on Bifurcation and Modal Coupling in Nonlinear Vibrations of Symmetric and Asymmetric Perforated Beams

Yue Liu[1,a], Shinichi Maruyama[1,b,*], Ken-ichi Nagai[1,c], Takao Yamaguchi[1,d], Chihiro Kamio[1,e]

Division of Mechanical Science and Technology, Graduate School of Science and Technology, Gunma University, Gunma, Japan

*Corresponding author

[a]<t192b605@gunma-u.ac.jp>, [b]<maruyama@gunma-u.ac.jp>, [c]<kennagai@gunma-u.ac.jp>, [d]<yamagme3@gunma-u.ac.jp>, [e]<chihiro. kamio@gunma-u.ac.jp>

Keywords: nonlinear vibrations, variable cross-section beam, perforated beam, bifurcation phenomenon

Abstract. Analytical results are presented on bifurcation and modal coupling in nonlinear vibrations of symmetrical and asymmetrical perforated beams in which both ends are clamped and subjected to lateral periodic force. In the analysis, the beam is divided into three segments, where the middle segment with a hole is modeled as a variable cross-section. The deflection of the beam is expanded with the mode shape function that is expressed with the product of truncated power series and trigonometric functions. Applying the Galerkin procedure, the nonlinear governing equation of the beam is reduced to a set of simultaneous nonlinear ordinary differential equation of motion in a multiple-degree-of-freedom system, by which nonlinear responses are obtained. The principal resonance of the lowest mode of the symmetrical beam is accompanied by the pitchfork bifurcation due to the sudden occurrence of super-harmonic resonance of the order-two of the 2^{nd} mode. In contrast, the principal resonance of the lowest mode of the asymmetrical beam is accompanied by the saddle-node bifurcation, which is perturbed from the pitchfork bifurcation, because of the loss of symmetry of the beam. Furthermore, as the asymmetricity of the beam increases, the bifurcation occurs at the lower frequency.

1. Introduction

In recent years, structure of mechanical or electronic devices have been more compact than before, and it is composed of a large number of thin elastic structural elements. Those elements have complex shapes and discontinuous cross-sections. When the thin beams are subjected to an external periodic excitation, large-amplitude resonance and nonlinear responses are easily generated. At the same time, due to the change in one of the system parameters, the modal coupling phenomenon may appear, accompanied by bifurcation, which will eventually cause a qualitative change in the dynamics of the entire system.

The subject of non-linear vibrations of structures has received much attention, at the same time, the internal resonance and bifurcation phenomena of structures during nonlinear vibration have also been extensively studied by researchers. C. H. Riedel and C. A. Tan [1] studied the coupled and forced responses of an axially moving strip with internal resonance. They found that the response of the vibration system has a 3 to 1 internal resonance between the first two transverse modes. C.M. Chin and A.H. Nayfeh [2] investigated internal resonance in hinged–clamped beams subject to a primary excitation in either its first or its second mode. They showed that the frequency of the second mode is approximately three times that of the first mode and hence a three-to-one internal resonance can be activated. X. Y. Mao et al. [3] analyzed the primary and the secondary resonance of a super-critically axially moving beam subjected to 3:1 internal resonance, the first-two modes are found to be coupled

Nomenclature		$u_{[n]}$	Axial displacement at the right-hand-side of the *n*-th segment
Symbols		w_{en}	Unknown time functions at nodes
L	Beam length	Z_{ni}	Mode shape functions
b	Beam width	$\{w_{en}\}$	A vector consists of w_{en}
$U(x,t)$	Axial displacement	$\{\bar{Z}_n\}$	A vector consists of Z_{ni} and its 1st-, 2nd-, and 3rd-order derivatives
$W(x,t)$	Deflection	$\bar{Z}_{ni}$	A component of $\{\bar{Z}_n\}$
P_s	Magnitude of static acceleration	$\delta_{i,f(k,l)}$	Kronecker-delta
P_d	Amplitude of periodic acceleration	$[Z_n]$	A matrix about $\bar{Z}_{ni}$
t	Time	$[D_n]$	A matrix consists of parameters of the *n*-th segment
A_n	Cross-sectional area	$\{\hat{b}\}$	Global nodal vector includes the nodal vectors $\{w_{en}\}$ of the all segments
ρ_n	Density	$\{\hat{d}\}$	Vector consists of axial displacement $u_{[n]}$ of all nodes
E_n	Young's modulus		
I_n	Moment of inertia of cross section	$\{\bar{b}\}$	Static deflection
Non-dimensional Symbols		$\{\tilde{b}\}$	Dynamic deflection
Δl	Distance from the hole to the center of the beam	$\tilde{\zeta}_j$	Linear natural modes of vibration
ξ_n	Local non-dimensional coordinate	$\omega_1, \omega_2, \omega_3$	First three natural frequencies
ω	Excitation frequency	w_{rms}	RMS value of deflection
τ	Time	b_{2rms}	RMS value of deflection of the 2nd mode
p_s	Magnitude of static acceleration	b_1, b_2	Normal coordinate of the lowest and 2nd mode
p_d	Amplitude of periodic acceleration	A_1, A_2	Fourier amplitudes of the lowest and 2nd mode
w_n	Deflection	ω_{bf}	Excitation frequency of bifurcation
n_{xn}	Axial force	*Abbreviations*	
s_{xn}	Slope	PF	Pitchfork bifurcation
m_{xn}	Bending moment	SN	Saddle-node bifurcation
q_{xn}	Shearing force	RMS	Root mean square value

by the internal resonance. J. L. Huang et al. [4] investigated the transverse nonlinear steady-state vibrations of the axially moving beam, in which they found that the beam has a three-to-one internal resonance between the first two modes, when it is subjected to a harmonic excitation. W.Y. Tseng and J. Dugundji [5] investigated nonlinear vibrations accompanied with snap-through of a buckled beam with fixed ends, in which principal-harmonic and super-harmonic resonances of the beam are obtained by analytically and experimentally. The critical and post-critical behavior of a non-conservative non-linear damped planar beam, undergoing statical and dynamical bifurcations, is analyzed by A. Di Egidio et al. [6]. According to a research of H. Akhavan, B. S. et al [7], the phenomenon of internal resonance due to modal coupling is studied in the non-linear piezoelectric small-scale beam and secondary branches due to bifurcations are found by using the shooting method. M. H. Ghayesh and

M. Amabili [8] investigated nonlinear dynamics of an axially moving Timoshenko beam, the system with a three-to-one internal resonance between the first two modes is found by Galerkin method employing 20 degrees of freedom. In the article by G. X. Wang et al. [9], they investigated nonlinear free vibration and 3:1 internal resonance of a hanging cantilever beam. Moreover, the results of an experimental investigation of non-linear one-to-one modal coupling in the dynamic response of cantilever beams excited by a periodic transverse base excitation are presented by C. L. Zaretzky and M. R. M. C. Da Silva [10]. K. Nagai and S. Maruyama et al. [11-12] investigated nonlinear vibrations of a post-buckled beam with an axial elastic constraint by experiment and numerical analysis, they confirmed the bifurcation behavior from the sub-harmonic responses of 1/3 order and of 1/2 order to the chaotic responses, and the final analytical results agreed well with experimental results. S. Maruyama and M. Hachisu et al. [13] investigated nonlinear vibrations of a post-buckled beam with a stepped section. The stepped beam is divided into a few number of segments and nonlinear and chaotic vibrations are numerically solved taking deflections, slope, bending moments, and shearing force as unknown time functions. The numerical results are also confirmed by experiments. S. Maruyama, T. Yamaguchi et al. [14] investigated chaotic vibrations due to internal resonance of 2nd and 3rd modes of an arch by experiment. F. Fontanela et al. [15] confirmed the two coupled beams with piecewise linear stiffness show bifurcations to localized solutions. In [16], bifurcation analysis is conducted for nonlinear vibrations of a composite cantilever beam under active control.

When large amplitude vibration response is induced in a thin beam, modal coupling between symmetrical and asymmetrical modes might appear accompanied by bifurcation. The modal coupling and bifurcation phenomena are sensitive to the asymmetricity of the beam, but those phenomena have not been clearly explained. Therefore, this paper presents numerical results on modal couplings in nonlinear vibrations of symmetrical or asymmetrical perforated beams. With increasing the asymmetricity of the perforated beam, change of the bifurcation is discussed in detail, where the asymmetric mode appears in the principal resonance of the lowest mode.

2. Procedure of Analysis

As shown in Fig. 1, a beam of which length L is clamped at the both ends. The x- and z-axes are introduced in the axial and lateral directions of the beam, respectively. The symbols $U(x,t)$ and $W(x,t)$ denote axial displacement and deflection, respectively. The beam is subjected to the static and periodic acceleration $P_s + P_d \cos\Omega t$. The four types of perforated beam are considered in this paper, which are shown in Fig. 2. The beams have a circular hole with the diameter half of the beam width b. The Model 1 is symmetric, i.e., the circular hole is located at the center of the beam. In contrast, the Models 2, 3, and 4 are asymmetric, i.e., the center of circular hole is located $\Delta l = 0.02L$, $0.06L$, and $0.12L$, respectively, apart from the center of the beam.

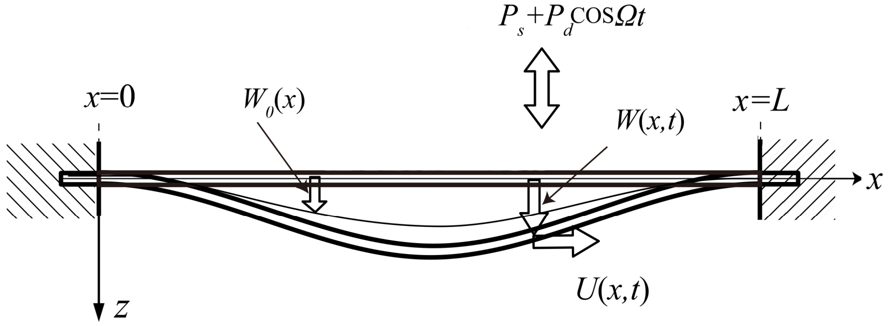

Fig. 1. Analytical model.

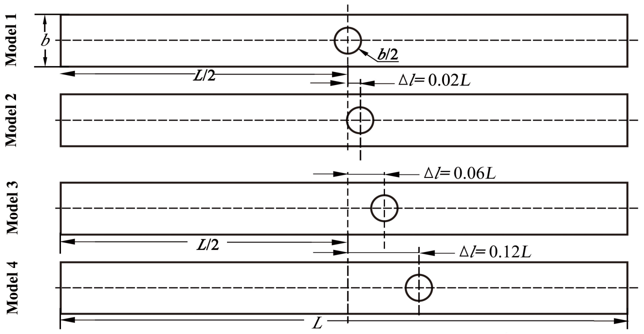

Fig. 2. Four models of beam.

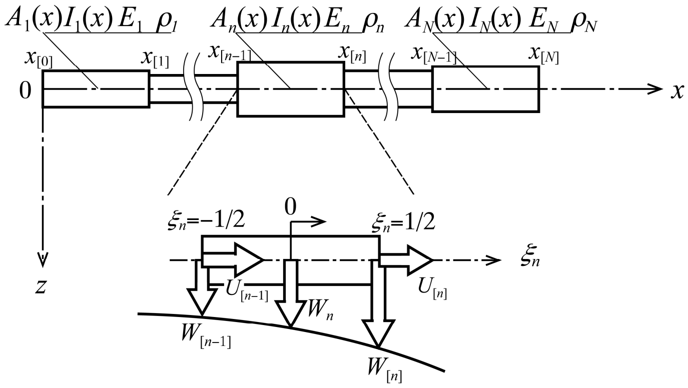

Fig. 3. Local coordinate system.

In the analysis, the beam is divided into three segments, two of which correspond to the parts with original rectangular cross section, while the other is the part with a hole in the range $L/2-b/2<x<L/2+b/2$ for the Model 1 and $L/2-b/2+\Delta l<x<L/2+b/2+\Delta l$ for the Models 2, 3, and 4. The local non-dimensional coordinate ξ_n is introduced for the *n*-th segment ($-1/2<\xi_n<1/2$) as shown in Fig. 3. The symbols A_n, ρ_n, E_n and I_n in Fig. 3 denote the cross-sectional area, density, Young's modulus and the cross-sectional moment of the *n*-th segment, respectively.

For sufficiently thin beams, the axial inertia, rotational inertia and shearing deformation can be neglected. Based on the Hamilton's principle, non-dimensional governing equation of motion is derived as shown in Eq. (1), in which the non-dimensional deflection, axial force, slope, bending moment, and shearing force are denoted as w_n, n_{xn}, s_{xn}, m_{xn} and q_{xn}, respectively. The symbol $u_{[n]}$ is axial displacement at the right-hand-side of each segment. Symbols p_s and p_d of Eq. (1) are the non-dimensional quantities of static and periodic acceleration, respectively. Symbols ω and τ are non-dimensional excitation frequency and time, respectively.

$$\begin{gathered}
\int_{\tau_0}^{\tau_1}\left\{\sum_{n=1}^{N}\left[\int_{-1/2}^{1/2}G_{w1}(w_n)\delta w_n d\xi_n+\left[q_{xn}\delta w_n\right]_{-1/2}^{1/2}-\left[d_n m_{xn}\delta w_n,_{\xi_n}\right]_{-1/2}^{1/2}\right]\right\}d\tau=0\\
G_{w1}\left(w_n\right)=d_n^{-1}\overline{\rho_n A_n}w_n,_{\tau\tau}-d_n n_{xn}w_n,_{\xi_n\xi_n}-d_n m_{xn},_{\xi_n\xi_n}-d_n^{-1}\overline{\rho}_n\overline{A}_n(p_s+p_d\cos\omega\tau)\\
n_{xn}=d_n\overline{E}_n\overline{A}_n\left(u_{[n]}-u_{[n-1]}\right)+\left(1/2\right)d_n^{\,2}\overline{E}_n\overline{A}_n\int_{-1/2}^{1/2}w_n,_{\xi_n}^{\;2}\,d\xi_n\\
m_{xn}=-d_n^2\overline{E}_n\overline{I}_n w_n,_{\xi_n\xi_n}\;;\quad s_{xn}=d_n w_n,_{\xi_n}\;;\quad q_{xn}=d_n n_{xn}w_n,_{\xi_{xn}}+d_n m_{xn},_{\xi_{xn}}
\end{gathered}\tag{1}$$

$$
\begin{aligned}
&w_n(\xi_n,\tau)=\{\zeta_n\}^T\{w_{en}\}=\sum_{j=1}^{8}w_{enj}(\tau)\zeta_{nj}(\xi_n),\{\zeta_n\}=\{\bar{Z}_n\}^T([D_n][Z_n])^{-1},\\
&\bar{Z}_{ni}=\sum_{l=1}^{2}\sum_{k=1}^{4}\delta_{i,f(k,l)}\left\{(2\xi_n)^{k-1}\cos(l-1)\pi(\xi_n+1/2)\right\},f(k,l)=4(l-1)+k
\end{aligned}
\tag{2}
$$

The deflection w_n of each segment is expressed with the linear combination of coordinate function ζ_n, by taking the nodal variables w_{en} as unknown time functions as shown in Eq. (2). The coordinate function ζ_n is defined by the linear combination of the mode shape functions Z_{ni} those are product of the truncated power series up to the 3rd-order and the trigonometric function. The coefficients of linear combination is appropriately chosen so that the w_n and its derivative up to the 3rd order at the both ends of segment are identical to the corresponding component of $\{w_{en}\}$. The vector $\{w_{en}\}$ consists of the nodal variables w_n, s_{xn}, m_{xn} and q_{xn} at both ends of the beam segment. $\{\bar{Z}_n\}$ is a vector consists of the mode shape functions, $\bar{Z}_{ni}$ is a component of $\{\bar{Z}_n\}$, the subscript *i* indicates the number of rows of $\{\bar{Z}_n\}$, and $\delta_{i,f(k,l)}$ is the Kronecker-delta. $[Z_n]$ is an 8×8 matrix consists of $\bar{Z}_{ni}$ and its 1st-, 2nd-, and 3rd-order derivatives, $[D_n]$ is an 8×8 matrix consists of parameters of the *n*-th segment. Introducing the global nodal vector $\{\hat{b}\}$ which includes the nodal vectors $\{w_{en}\}$ of the all segments, and the vector $\{\hat{d}\}$ which consists of axial displacement $u_{[n]}$ of all nodes, and applying the Galerkin procedure, the nonlinear governing equation of the beam is reduced to a set of ordinary differential equations as follows.

$$
\sum_q \hat{B}_{pq}\hat{b}_{q,\tau\tau}+\sum_q \hat{C}_{pq}\hat{b}_q+\sum_q\sum_v \hat{D}_{pqv}\hat{b}_q\hat{d}_v+\sum_v\sum_q \hat{D}_{pvq}\hat{d}_v\hat{b}_q+\sum_q\sum_r\sum_s \hat{E}_{pqrs}\hat{b}_q\hat{b}_r\hat{b}_s-\hat{F}_p-\hat{G}_p(p_s+p_d\cos\omega\tau)=0 \tag{3}
$$

$$
\sum_v \hat{C}_{tv}\hat{d}_v+\sum_r\sum_s \hat{D}_{trs}\hat{b}_r\hat{b}_s-\hat{F}_t=0 \qquad p,q,r,s=1,2,\cdots,4(N+1),t,v=4(N+1)+1,4(N+1)+2,\cdots,5(N+1) \tag{4}
$$

Based on Eq. (4) , the axial displacement of each node $\{\hat{d}\}$ can be expressed as the functions of $\{\hat{b}\}$, and then substituting it into Eq. (3), the equation of motion can be expressed only by unknowns $\{\hat{b}\}$. The node vector $\{\hat{b}\}$ is separated into $\{\bar{b}\}$ of the static deflection and the dynamic deflection $\{\tilde{b}\}$. By ignoring the time-varying term, the static deflection $\{\bar{b}\}$ caused by the static lateral acceleration and the initial axial displacement is obtained. Next, the ordinary differential equation is converted into the equation of the dynamic variable $\{\tilde{b}\}$ measured from the static equilibrium position. Furthermore, the ordinary differential equations are transformed to the standard form in terms of normal coordinates b_i corresponding to the linear natural modes of vibration $\tilde{\zeta}_j$ at the static equilibrium position of the beam. Dynamic responses can be calculated with the harmonic balance method and the Runge-Kutta-Gill numerical integration method.

3. Results and Discussion

In the following results, frequency response and time histories are obtained numerically for model 1~4 under the static acceleration $p_s=271$ and amplitude of periodic acceleration $p_d=3000$. The responses of deflection are measured at $\xi=0.25$.

3.1 Symmetric beam

Figure 4 shows the analytical results of frequency response curve of Model 1. In the frequency response curve, the black and gray curves show the stable and unstable periodic responses, respectively, calculated by the harmonic balance method. The red and blue curves represent the forward sweeping solution and the downward sweeping solution which are calculated by Runge-Kutta-Gill method, respectively. The symbols ω_1, ω_2, and ω_3 in the figures represent the first three natural frequencies of each model, respectively. Moreover, symbols (1:1) and (3:1) represent the principal resonance of the lowest mode and 3rd mode, respectively. The (1:2) and (1:3) respectively represent the super-harmonic resonances of order 2 and 3 of the lowest mode, while (1:1/2) and (1:1/3) represent sub-harmonic resonance of order 1/2 and 1/3 of the lowest mode.

The principal resonance of the lowest mode (1:1), the sub-harmonic resonance of order 1/2 of the lowest mode (1:1/2), and the principal resonance of the 3rd mode (3:1) of Model 1 in Fig. 4 show frequency response curve corresponding to almost hardening restoring force characteristics.

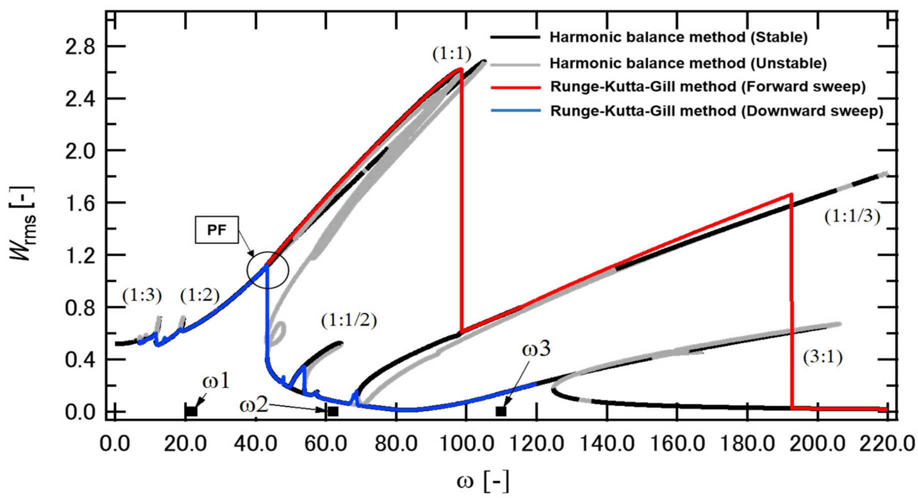

Fig. 4. Frequency response curve (Model 1).

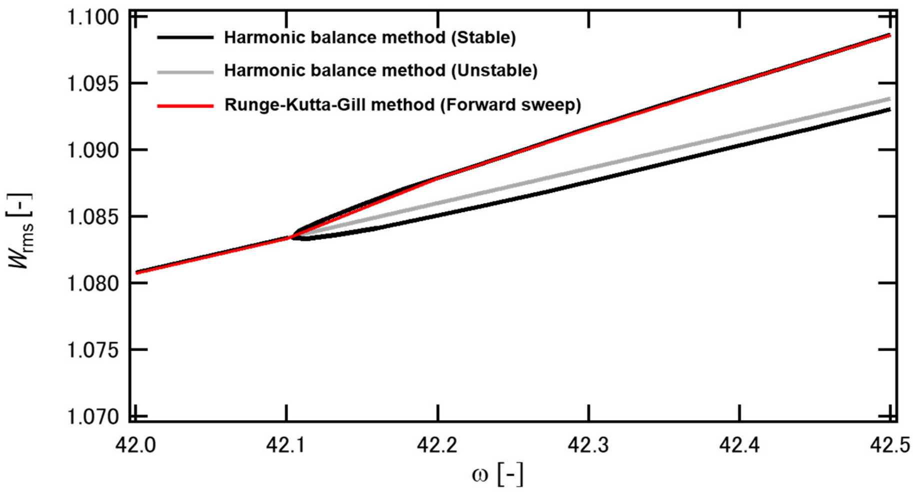

Fig. 5. Partial magnification of frequency response curve (Model 1).

Figure 5 shows partial magnification of the black circular part of frequency response curve in Fig. 4. It can be seen that the branch of periodic response (1,1) bifurcates to three branches at excitation frequency $\omega = 42.11$, and the result of direct numerical integration follows one of the stable branches. It also can be confirmed that there is a pitchfork (PF) bifurcation in the figure.

Figure 6 shows the frequency response curve of normal coordinate b_2 of 2nd mode. Figure 7 is the enlarged figure of the black circle in Fig. 6 around the bifurcation point. In the frequency band ($42 < \omega < 100$) corresponding to the large amplitude part of the (1:1) resonance response, the amplitude of the 2nd mode increases sharply after the bifurcation, while the amplitude of b_{2rms} of the 2nd mode is zero before the bifurcation.

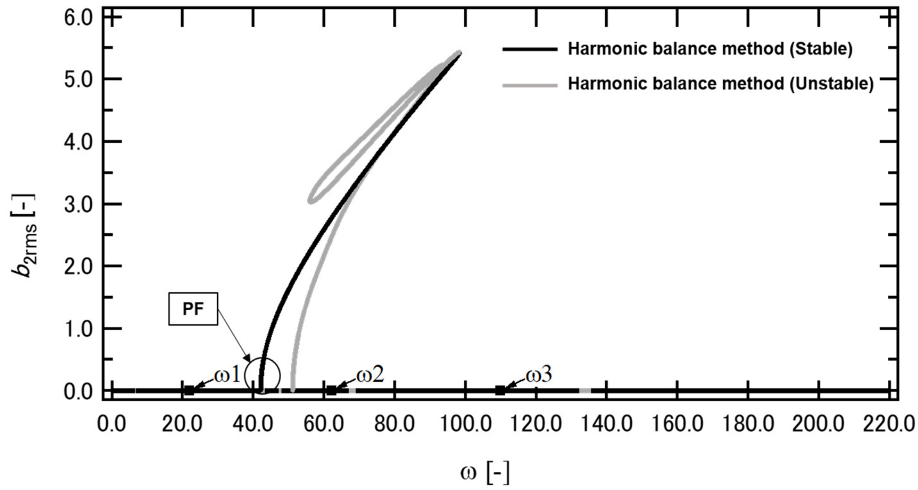

Fig. 6. Frequency response curve of 2nd mode (Model 1).

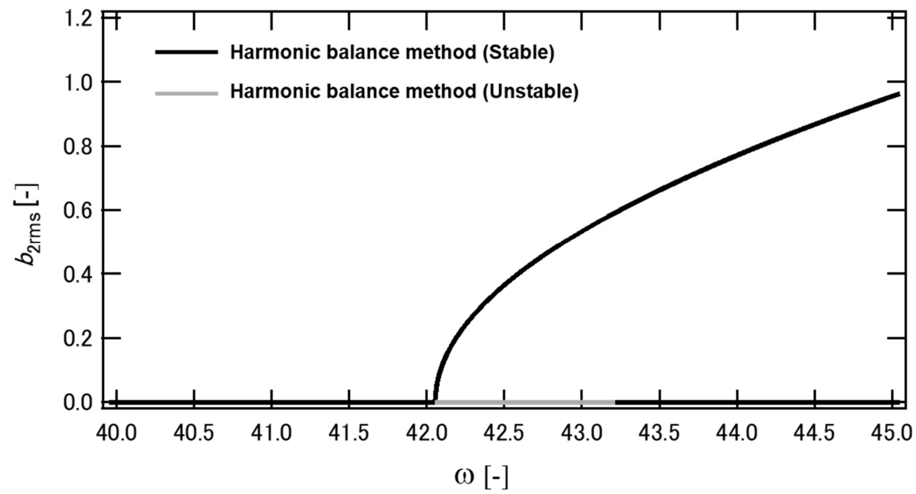

Fig. 7. Partial magnification of frequency response of 2nd mode (Model 1).

Figure 8 represents the time histories of normal coordinates b_1 and b_2 of the lowest mode and 2nd mode, respectively. Figs. 8 (a) and (b) are the time histories before and after the PF bifurcation, their corresponding excitation frequencies are $\omega = 40$ and $\omega = 50$, respectively. According to the Figs. 8 (a) and (b), the peak value of b_1 is much larger than that of b_2 before the PF bifurcation at $\omega = 40$. However, compared to before the PF bifurcation at $\omega = 40$, although the peak value of b_1 is hardly changed after the PF bifurcation at $\omega = 50$, the peak value of b_2 is increased largely.

Through the FFT analysis of the time histories of Model 1 before and after the PF bifurcation, the Fourier spectra of Model 1 can be obtained in Figs. 9 (a) and (b), respectively. The symbols A_1 and A_2 represent the Fourier spectra amplitudes of the lowest mode and 2nd mode, respectively. In Fig.9 (a), before the PF bifurcation, the curves of A_1 and A_2 have the largest peak value at the excitation frequency $\omega = 40$, i.e., principal resonance component of the lowest mode has a great contribution to the response at $\omega = 40$. However, according to the curves A_1 and A_2 of Fig. 9 (b), after the PF bifurcation at excitation frequency $\omega = 50$, the peak value of A_1 still appears at excitation frequency $\omega = 50$, but the peak value of A_2 appears at twice of the excitation frequency 2ω ($2\omega = 100$), i.e., not only the principal resonance component of the lowest mode at $\omega = 50$, the twice harmonic component of the 2nd mode at $2\omega = 100$ also has a great contribution to the vibration response. It can be confirmed that the 2nd mode is generated with super-harmonic resonance after the PF bifurcation. Therefore, this bifurcation is due to the two to one internal resonance caused by the modal coupling between the lowest and the 2nd modes of vibration.

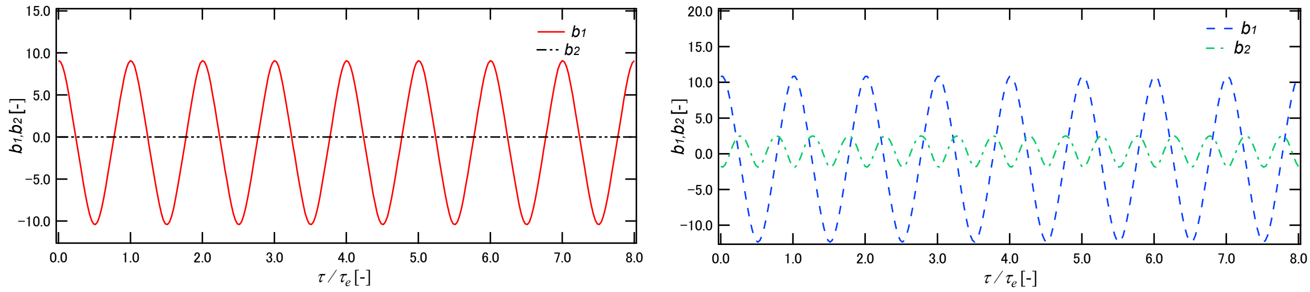

(a) before the bifurcation ($\omega = 40$) (b) after the bifurcation ($\omega = 50$)

Fig. 8. Time histories (b_1 and b_2 of Model 1).

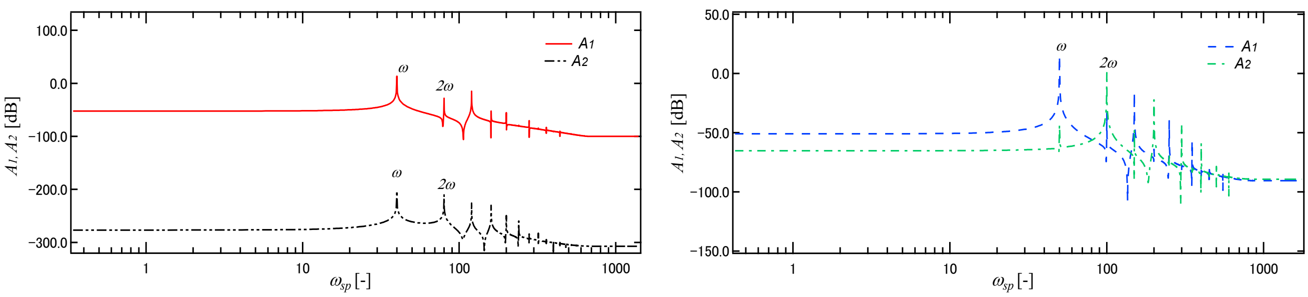

(a) before the bifurcation ($\omega = 40$) (b) after the bifurcation ($\omega = 50$)

Fig. 9. Fourier spectra (A_1 and A_2 of Model 1).

3.2 Asymmetric beam

Through analyzing the numerical calculation results of Model 2, the frequency response curves are obtained in Fig. 10. According to Fig. 10, the principal resonance of the lowest mode (1:1), the sub-harmonic resonance of order 1/2 of the lowest mode (1:1/2), and the principal resonance of the 3rd mode (3:1) of Model 2 show almost hardening restoring force characteristics. In addition, different with Model 1, the principal resonance of the 2nd mode (2:1) of Model 2 appears, indicating that the asymmetrical position of the hole enables the 2nd mode resonance to appear, and it also shows almost hardening restoring force characteristics. Moreover, Figure 11 shows partial magnification of the black circular part of frequency response curve in Fig. 10. It can be seen that a saddle-node (SN) bifurcation occurs at excitation frequency $\omega = 42.08$ in Fig. 11. Next, Figure 12 shows frequency response curve of normal coordinate b_2 of 2nd mode, while Fig. 13 shows the enlarged the black circle of Fig. 12

around the bifurcation point. Because of the asymmetrical position of the hole, the 2nd mode is continuously induced even before the bifurcation, and the PF bifurcation is perturbed to become the SN bifurcation.

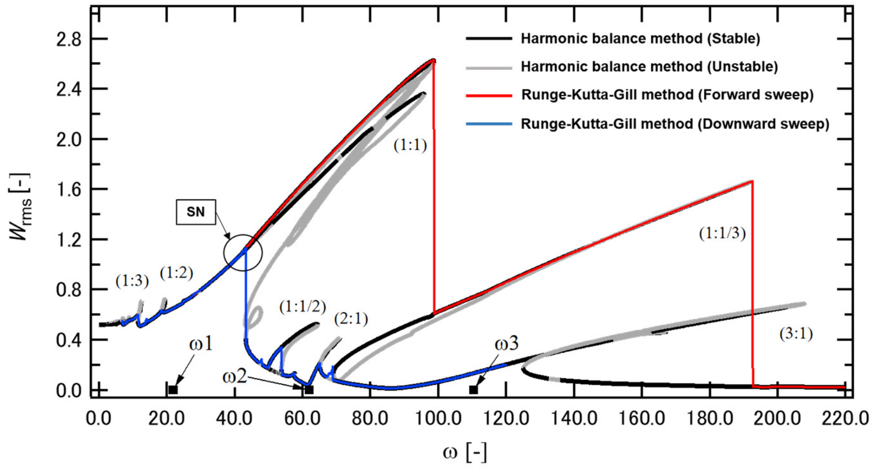

Fig. 10. Frequency response curve (Model 2).

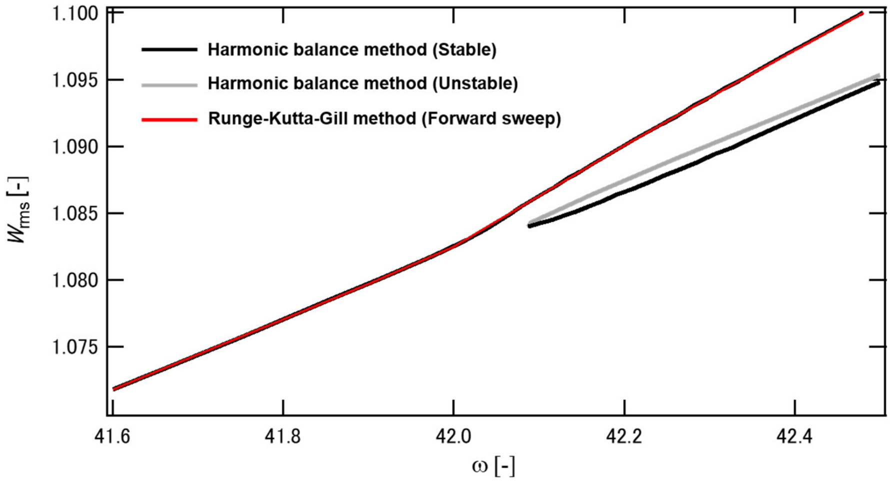

Fig. 11. Partial magnification of frequency response curve (Model 2).

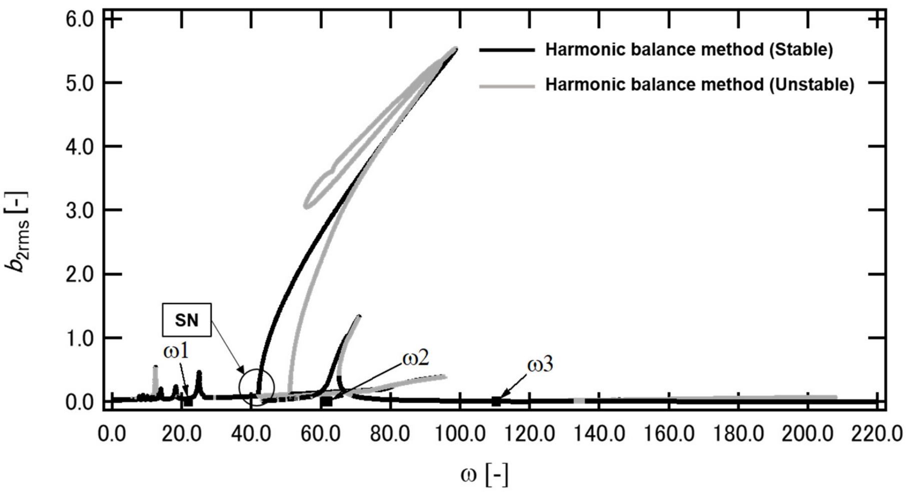

Fig. 12. Frequency response curve of 2nd mode (Model 2).

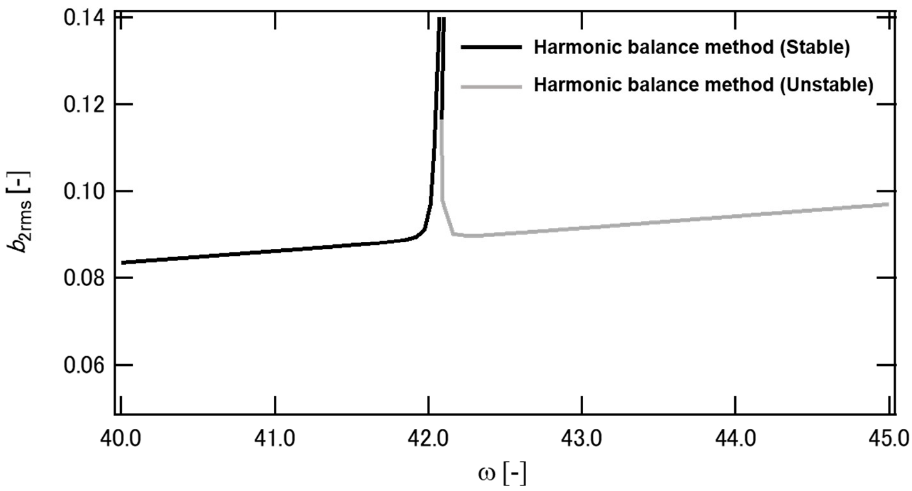

Fig. 13. Partial magnification of frequency response of 2nd mode (Model 2).

The time histories and Fourier spectra of Model 2 are compared with those of Model 1, respectively, where Figs. 14 (a) and (b) represent the time histories of b_1 and of b_2 of Model 2 before and after the PF bifurcation, respectively. Figs. 15 (a) and (b) represent Fourier spectra of b_1 and b_2 of Model 2 before and after the PF bifurcation, respectively.

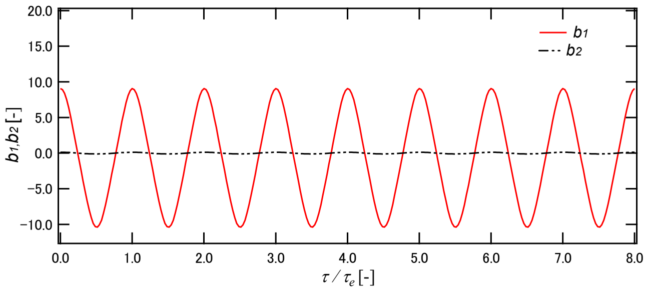

(a) before the bifurcation ($\omega = 40$)

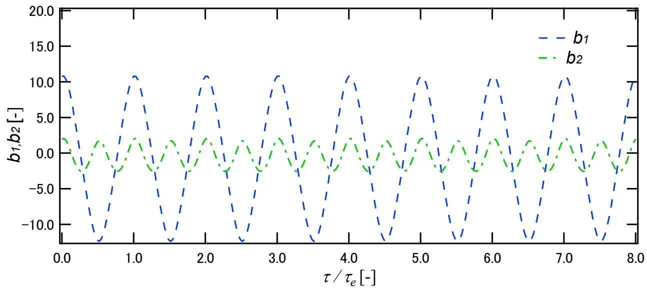

(b) after the bifurcation ($\omega = 50$)

Fig. 14. Time histories (b_1 and b_2 of Model 2).

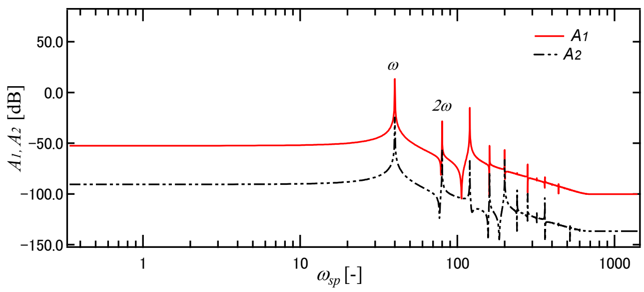

(a) before the bifurcation ($\omega = 40$)

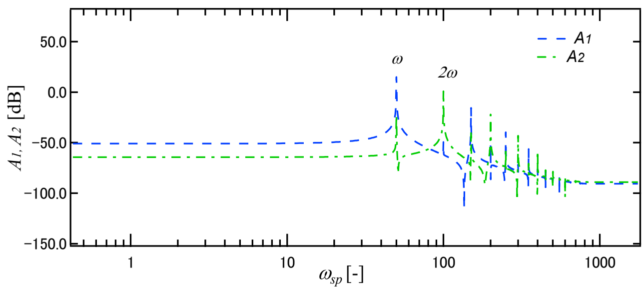

(b) after the bifurcation ($\omega = 50$)

Fig. 15. Fourier spectra (A_1 and A_2 of Model 2).

Firstly, according to Fig. 8 (a), time history of b_2 of Model 1 hardly changes with time, i.e., the values of b_2 approach zero before the bifurcation at $\omega = 40$. On the contrary, in Fig.14 (a), the amplitude of b_2 of Model 2 is non-zero before the bifurcation at $\omega = 40$. Figure 15 (a) is obtained by performing FFT on the time histories of Fig. 14 (a). It is found from the observation of Figs. 9 (a) and 15 (a) that the maximum amplitude A_2 of Model 2 is greater than that of Model 1 before the bifurcation at $\omega = 40$. This indicates that the position of the hole affects the symmetry of the model, i.e., the 2nd mode of symmetric beam before the bifurcation is never induced, however, in the case of an asymmetric beam, it will be slightly induced before the bifurcation of the 2nd mode. Moreover, according to the curve A_2 of Fig.15 (b), after the bifurcation, it also can be confirmed that the peak of b_2 appears at excitation frequency ($2\omega = 100$), i.e., when the model is asymmetric, the twice harmonic component of the 2nd mode at $2\omega = 100$ also have a great contribution to the vibration response.

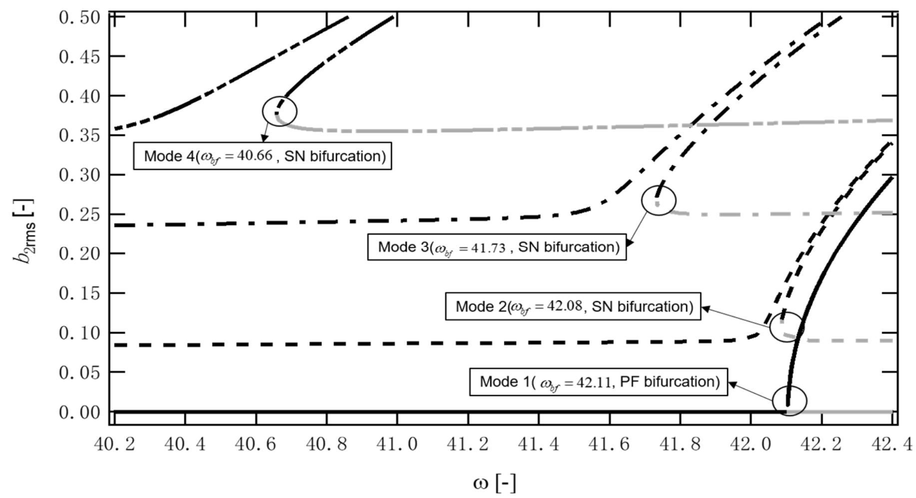

Fig. 16. Comparison of frequency response curves of 2nd mode for four models.

In order to further investigate the influence of asymmetricity on the bifurcation of the beam, i.e., the effect of Δl on the bifurcation, the results of Model 3 and 4 are obtained by numerical calculation. The frequency response curves of Model 1~4 are compared in Fig. 16, in which the ω_{bf} represents the value of the excitation frequency when the bifurcation occurs.

According to Fig. 16, for Models 1~4, due to the increase in Δl, the amplitude of b_{2rms} for corresponding model is increasing and the locations of bifurcations are shifted towards the lower frequency. It is considered that the asymmetry of the model increases, i.e., the value of Δl is increased, internal resonance due to mode coupling between the lowest mode and the 2nd mode is more likely to occur. Hence, the 2nd mode is generated with super-harmonic resonance earlier, the bifurcation occurs at the lower frequency.

4. Conclusions

Through the above analyses, the following conclusions are obtained:

(1) When the hole is at the center of the beam, the branch of periodic response the principal resonance of the lowest mode bifurcates to three branches of which two stable responses are accompanied by super-harmonic resonance of order-two of the 2nd mode. Due to modal coupling with super-harmonic resonance of order-two of the 2nd mode, the PF bifurcation appears along the principal resonance response of the lowest mode.

(2) When the hole is apart from the center of the beam, the loss of symmetry leads to the appearance of the SN bifurcation. The reason is that, because of the asymmetrical position of the hole, the 2nd mode is continuously induced before and after bifurcation, which perturbs the PF bifurcation to become the SN bifurcation.

(3) When the asymmetricity of the beam increases by changing the position of the hole from the center, the bifurcation occurs at the lower frequency.

References

[1] C. H. Riedel, C. A. Tan, “Coupled, forced response of an axially moving strip with internal resonance”, ***International Journal of Non-Linear Mechanics***, Vol. 37, No. 1, pp. 101-116, 2002.

[2] C.M. Chin, A.H. Nayfeh. “Three-to-one internal resonances in hinged–clamped beams”, ***Nonlinear Dynamics***, Vol. 12, No. 2, pp. 129–154, 1997.

[3] X. Y. Mao, H. Ding, L. Q. Chen, “Forced vibration of axially moving beam with internal resonance in the supercritical regime”, ***International Journal of Mechanical Sciences***, Vol.131, pp. 81-94, 2017.

[4] J. L. Huang, R. K. L. Su, W. H. Li, et al, “Stability and bifurcation of an axially moving beam tuned to three-to-one internal resonances”, ***Journal of Sound and Vibration***, Vol. 330, No. 3, pp. 471-485, 2011.

[5] W.Y. Tseng, J. Dugundji, “Nonlinear vibrations of a buckled beam under harmonic excitation”, ***ASME Journal of Applied Mechanics***, Vol. 38, pp. 467–476, 1971.

[6] A. Di Egidio, A. Luongo, A. Paolone, “Linear and non-linear interactions between static and dynamic bifurcations of damped planar beams”, ***International Journal of Non-Linear Mechanics***, Vol. 42, No. 1, pp. 88-98, 2007.

[7] H. Akhavan, B. S. Roody, Ribeiro P, et al, “Modes of vibration, stability and internal resonances on non-linear piezoelectric small-scale beams”, ***Communications in Nonlinear Science and Numerical Simulation***, Vol. 72, pp. 88-107, 2019.

[8] M. H. Ghayesh, M. Amabili, “Nonlinear dynamics of an axially moving Timoshenko beam with an internal resonance”, ***Nonlinear Dynamics***, Vol. 73, No. 1, pp. 39-52, 2013.

[9] G. X. Wang, H. Ding, L. Q. Chen, “Dynamic effect of internal resonance caused by gravity on the nonlinear vibration of vertical cantilever beams”, ***Journal of Sound and Vibration***, Vol. 474: 115265, 2020.

[10] C. L. Zaretzky, M. R. M. C. Da Silva, “Experimental investigation of non-linear modal coupling in the response of cantilever beams”, ***Journal of Sound and Vibration***, Vol. 174, No. 2, pp. 145-167, 1994.

[11] K. Nagai, S. Maruyama, K. Sakaimoto and T. Yamaguchi, “Experiment on chaotic vibrations of a post-buckled beam with an axial elastic constraint”, ***Journal of Sound and Vibration***, Vol.304, pp.541-555, 2007.

[12] S. Maruyama, K. Nagai, T. Yamaguchi and K. Hoshi, “Contribution of multiple vibration modes to chaotic vibrations of a post-buckled beam with an axial elastic constraint”, ***Journal of System Design and Dynamics***, Vol. 2 No. 3, pp.738-749, 2008.

[13] S. Maruyama, M. Hachisu, K. Nagai, T. Yamaguchi, “Analysis and experiments on nonlinear vibrations of a post-buckled beam with a stepped section”, ***Journal of Mechanical and Electrical Intelligent System***, Vol. 3, No. 1, pp. 10-15, 2020.

[14] S. Maruyama, T. Yamaguchi, K. Nagai, “Experiments on chaotic vibrations of an arch deformed by an initial axial displacement”, ***Journal of Technology and Social Science***, Vol. 1, No. 2, pp. 12-24, 2017.

[15] F. Fontanela, A. Vizzaccaro, J. Auvray, et al. “Nonlinear vibration localisation in a symmetric system of two coupled beams”, ***Nonlinear dynamics***, Vol.103, No. 4, pp. 3417-3428, 2021.

[16] M. Sayed, A. A. Mousa, D. Y. Alzaharani, et al. “Bifurcation analysis of a composite cantilever beam via 1: 3 internal resonance”, ***Journal of the Egyptian Mathematical Society***, Vol.28, No. 1, pp. 1-21, 2020.